

GT 2007-27990

DEVELOPMENT AND APPLICATION OF AN EIGHT-STEP GLOBAL MECHANISM FOR CFD AND CRN SIMULATIONS OF LEAN-PREMIXED COMBUSTORS

Igor V. Novosselov

Philip C. Malte[‡]

Energy and Environmental Combustion Laboratory, Department of Mechanical Engineering
University of Washington, Box 352600, Seattle, WA 98195-2600

ABSTRACT

In this paper, the development of an eight-step global chemical kinetic mechanism for methane oxidation with nitric oxide formation in lean-premixed combustion at elevated pressures is described and applied. In particular, the mechanism has been developed for use in computational fluid dynamics (CFD) and chemical reactor network (CRN) simulations of combustion in lean-premixed gas turbine engines. Special attention is focused on the ability of the mechanism to predict NO_x and CO exhaust emissions. Applications of the eight-step mechanism are reported in the paper, all for high-pressure, lean-premixed, methane-air (or natural gas-air) combustion.

The eight steps of the mechanism are as follows:

1. Oxidation of the methane fuel to CO and H_2O .
2. Oxidation of the CO to CO_2 .
3. Dissociation of the CO_2 to CO.
4. Flame NO formation by the Zeldovich and nitrous oxide mechanisms.
5. Flame NO formation by the prompt and NNH mechanisms.
6. Post-flame NO formation by equilibrium H-atom attack on equilibrium N_2O .
7. Post-flame NO formation by equilibrium O-atom attack on equilibrium N_2O .
8. Post-flame Zeldovich NO formation by equilibrium O-atom attack on N_2 .

INTRODUCTION

Computational fluid dynamics (CFD) modeling of lean-premixed gas turbine combustors has relied on the use of global chemical kinetic mechanisms for prediction of heat release. This includes the use of mechanisms of one to four steps drawn from the combustion literature, e.g. [1,2,3,4]. Most of the mechanisms do not include a reverse step for carbon monoxide; thus it is difficult to obtain convergence of CO in the burnout zone of the combustor and the ability to predict CO exhaust emission is lost. Furthermore, the global mechanisms do not include nitric oxide (NO) kinetics. Although CFD packages include post-processing for NO, especially for thermal Zeldovich NO, the details of flame-formed NO are lacking. Flame-formed NO lies at the heart of NO_x and its control for advanced gas turbine engines with single-digit emissions.

Our goal has been to develop a global mechanism that permits the prediction of part per million emissions of CO and NO_x as well as provides reasonable results for heat release and patterns for temperature and major species in the lean-premixed combustor. Focus is on the industrial combustor – thus, the pressure range of our mechanism is 5-20 atm, and the inlet air temperature is set accordingly. The mechanism is valid for fuel-air equivalence ratios (ϕ) from about 0.45 to 0.75, and for mean residence times from slightly greater than blowout to full combustor time. The fuel is methane or natural gas sufficiently high in methane so that it can be reasonably simulated as methane.

The eight-step mechanism builds on a five-step mechanism we previously developed [5]. The five-step mechanism used two NO steps, one for the flame zone and one for the post-flame zone, and was restricted to single pressures, whereas the

[‡] corresponding author: malte@u.washington.edu

eight-step mechanism has variable pressure and five NO steps. Also, the database used for the development of the five-step mechanism was smaller than that used for the eight-step mechanism.

The balance of the paper is divided into the following sections:

- Discussion of the key points about NO formation in lean-premixed combustion, which uses results from our CFD modeling of a generic can-type gas turbine combustor.
- Development of the eight-step mechanism, including a discussion of the database used for obtaining the mechanism, and a listing and explanation of the mechanism.
- Application of the eight-step mechanism in CFD modeling of an experimental bluff body combustor.
- Application of the eight-step mechanism in CRN modeling of a test rig gas turbine combustor.

NO FORMATION IN LEAN-PREMIKED COMBUSTION

Prior to discussing the development of the eight-step mechanism, it is helpful to briefly review the formation of NO in lean-premixed combustion. (Please note the terms “NO formed” and “NO_x emitted” can be used interchangeably, since a fraction of the NO formed is oxidized to NO₂ within the combustor and engine. Thus, the computation of NO formed is equivalent to NO_x emitted.)

For this discussion a generic, can-type, swirl-stabilized, air-back-sided cooled, lean-premixed combustor for the industrial gas turbine engine is assumed. A commercial CFD package (Fluent 6.2) is used to solve a 2-D, axi-symmetric rendition of the combustor. Details are given in the PhD thesis of Novosselov [6]. The upper, forward part of the combustor is shown in the CFD results pictured below in Figures 1 through 8. The eight-step mechanism provides the global reactions and rates. For each reaction step the slower of two rate choices is selected by the CFD: either the chemical kinetic rate (as provided by the eight-step mechanism) or the mixing controlled rate as calculated by the eddy breakup model [7]. In this case, since the combustion is premixed, the reactants-products eddy breakup rate, rather than the fuel-air rate, is selected. The first reaction step is significantly affected by this choice; that is, the initial oxidation of the methane to water vapor and CO tends to be mixing controlled in these combustors, except in regions of intense shear. The oxidation of CO can experience either kinetic or mixing control, though the tendency is kinetic control. NO formation is kinetically controlled.

Figure 1 shows the velocity vectors, and Figure 2 shows the temperature contours of the combustor. Also seen is the flame structure (Figure 3 and Figure 4). Swirled air-fuel mixture exits the main premixer-injector shown above the centerline of the combustor. The premixer-injector is also solved in CFD. For the results plotted in Figures 1 to 8, a uniform fuel-air ratio is assumed across the premixer. Centrifugal force pulls the premixed stream radially outward after it leaves the premixer, and the mixture is ignited by

mixing with the recirculation zones: mainly with the large on-axis recirculation zone but also by the smaller dome recirculation zone. The methane destruction rate (Figure 3) and the CO concentration (Figure 4) indicate the location of the flame zone; this is the main region of non-equilibrium chemical reaction. This combustor operates very lean: the phi of the main premixer-injector is 0.475, and that of the centerline pilot (which is premixed) is taken as 1/2 of this (i.e., 50% pilot is assumed in this case). This results in a relatively low peak temperature: 1710 K. Pressure is 16 atm.

Figures 5-8 show how and where the NO forms. Under the conditions represented, about 50% of the NO forms via the Zeldovich and nitrous oxide mechanisms within the flame zone (Figure 5), and about 25% forms in the flame zone by the prompt and NNH mechanisms (Figure 6). The mechanisms are listed in Table 1. The lumping of mechanisms together is done on the basis of where they are active in the flame zone: the prompt-NNH NO forms earlier in the flame zone than the Zeldovich-nitrous oxide NO. Furthermore, the prompt-NNH NO has the greatest maximum rate: however, since its region of impact is not as large as the Zeldovich-nitrous oxide NO, its contribution is about one-half that of the Zeldovich-nitrous oxide NO. The NO formed within the flame zone is termed non-thermal in order to distinguish it from thermal NO formed in the post-flame zone, which assumes the free radical species such as O-atom, H-atom, and OH-radical are at local thermo-chemical equilibrium condition. In the flame zone, however, the free radicals are at significantly greater concentrations, termed non-equilibrium or super-equilibrium. This drives the rates of NO formation to high levels within the flame zone. Thus, it is important to maintain the flame zone as thin as practically feasible in order to curtail NO formation in a single-digit emission lean-premixed combustor. Globalizing the Zeldovich and nitrous oxide reactions into one step for the flame zone, and the prompt and NNH reactions into another step is shown in the next section.

The NO formation is brought to 100% by noting that 25% is formed by the thermal steps in the post-flame zone of the combustor (Figure 7 and Figure 8). Although the maximum rates of thermal NO formation are 2-3 orders of magnitude less than the maximum rates of NO formation within the flame zone, since the post-flame expanse of the thermal NO formation is large relative to the flame zone, its contribution sums up to about 25%. Figure 8 shows the thermal Zeldovich NO, which is the textbook method of calculating NO formation, e.g., see [8]. However, under the present conditions, there is a second essentially equal contributor to post-flame thermal NO: thermal nitrous oxide NO (Figure 7), which assumes that N₂O and O, both at local equilibrium concentration, react to form NO.

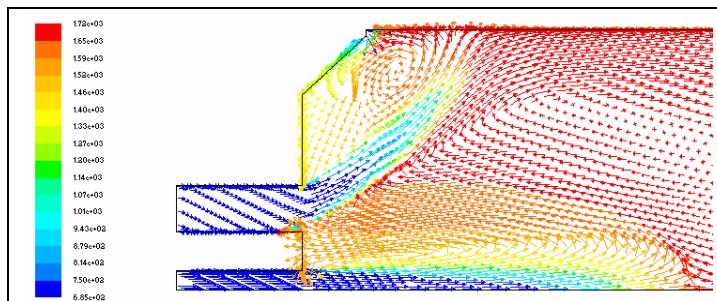


Figure 1. Vectors of velocity colored by temperature.

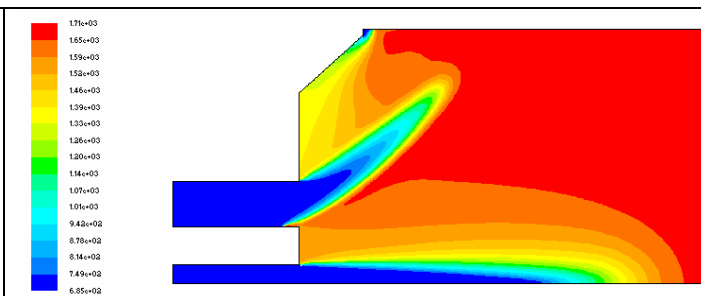


Figure 2. Temperature contour plot. Maximum is 1710 K.

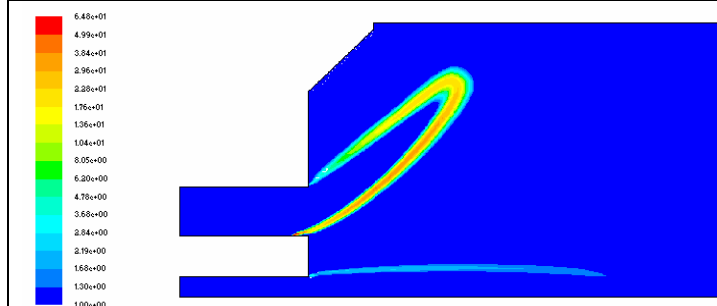


Figure 3. Rate of methane destruction reaction. Maximum rate is 65 kmol/m³/s.

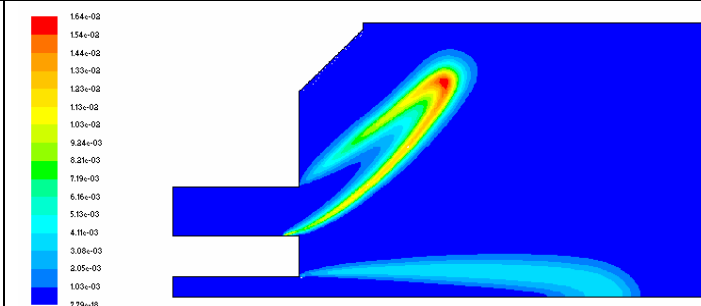


Figure 4. Mole fraction of CO. Maximum is 0.016 kmolCO/kmol total.

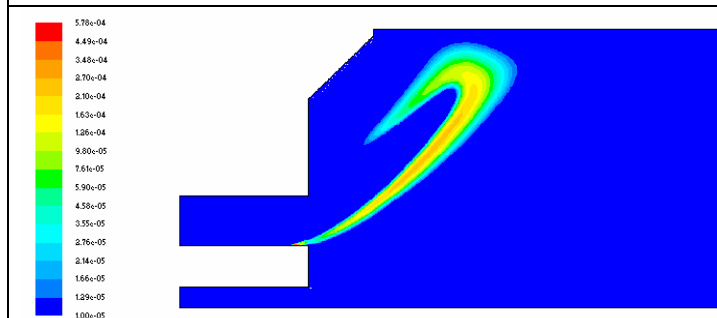


Figure 5. Rate of NO formation via non-thermal Zeldovich and nitrous oxide mechanisms (global step 4). Maximum rate is 5.78e-4 kmol/m³/s.

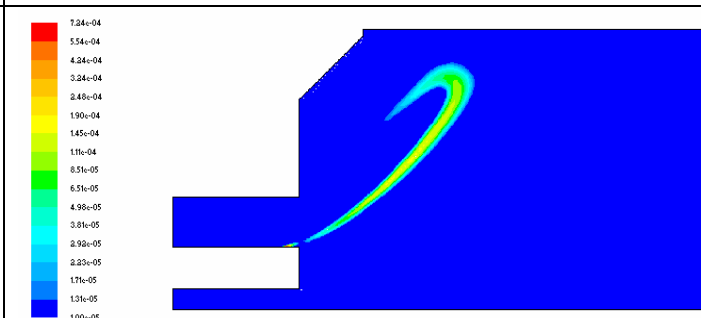


Figure 6. Rate of NO formation via prompt and NNH mechanisms (global step 5). Maximum rate is 7.25e-4 kmol/m³/s.

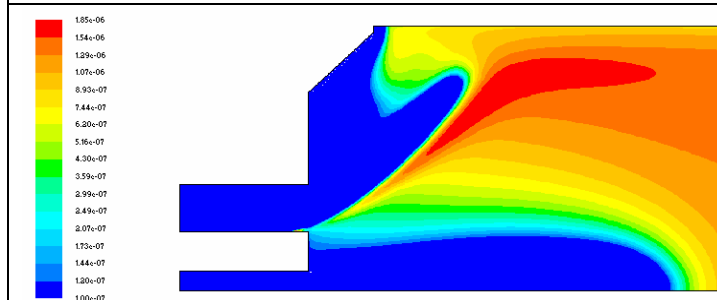


Figure 7. Rate of NO formation via thermal nitrous oxide mechanism assuming O-atom and N₂O equilibrium (global step 7). Maximum rate is 1.85e-6 kmol/m³/s.

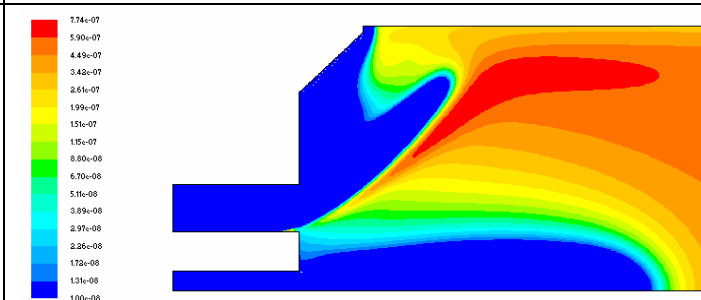


Figure 8. Rate of NO formation via thermal Zeldovich mechanism assuming equilibrium O-atom (global step 8). Maximum rate is 7.74e-7 kmol/m³/s.

Table 1. NO mechanisms and formation rates for lean-premixed combustion.

Zeldovich mechanism	
Rxn 1	$N_2 + O \Rightarrow NO + N$
Rxn 2	$N + O_2 \Rightarrow NO + O$
Rxn 3	$N + OH \Rightarrow NO + H$
Rate	$d[NO]/dt = 2k_1[N_2][O]$
Nitrous oxide mechanism	
Rxn 4	$N_2 + O + M \Rightarrow N_2O + M$
Rxn 5	$N_2O + O \Rightarrow NO + NO$
Rxn 6	$N_2O + H \Rightarrow NO + NH$
Note	Under lean-premixed combustion, quantitative oxidation of NH to NO is assumed.
Note	Several reactions [6], not shown here, convert N_2O back to N_2 .
Rate	$d[NO]/dt = 2k_5[N_2O][O] + 2k_6[N_2O][H]$
Prompt NO	
Rxn 7	$N_2 + CH \Rightarrow HCN + N$
Note	Under lean-premixed combustion, quantitative oxidation of HCN and N to NO is assumed.
Note	N reacts to NO by Rxn's 2 and 3.
Rate	$d[NO]/dt = 2k_7[N_2][CH]$
NNH mechanism	
Rxn 8	$N_2 + H \Rightarrow NNH + H$
Rxn 9	$N_2 + H + M \Rightarrow NNH + M$
Rxn 10	$NNH + O \Rightarrow NO + NH$
Rxn 11	$NNH + O \Rightarrow N_2O + OH$
Note	As noted above, the oxidation of NH to NO is assumed quantitative
Note	Several reactions [6], not shown here, convert NNH back to N_2 .
Note	The NO rate for the NNH chemistry does not include reaction 11.
Rate	$d[NO]/dt = 2k_{10}[NNH][O]$

DEVELOPMENT AND EXPLANATION OF THE EIGHT-STEP MECHANISM

The database used to generate the eight-step mechanism began with two high pressure jet stirred reactor (JSR) experiments, one at the University of Washington by Rutar [9] for pressures up to 6.5 atm, and the other at the Swiss Federal Institute of Technology by Bengtsson [10] for pressures up to 20 atm. The fuel in each study was methane. Rutar and Malte [11] compared both sets of experiments to simple chemical reactor network modeling, assuming two PSRs in series (i.e., perfectly stirred reactors) for the JSR of Rutar, and a PSR followed by a PFR (plug flow reactor) for the JSR of Bengtsson. The GRI 3.0 mechanism [12] was used for both JSRs. The volume of PSR1 relative to that of PSR 2 of the Rutar JSR depended on the experimental Damköhler number. For the Bengtsson JSR the PSR and PFR volumes were fixed as 88 and 12%, respectively, of total reactor volume. Experimental temperatures were used.

The modeling results were found to compare very favorably with the experimental results for CO, NO_x , and N_2O . The modeling also provided estimates of the free radical concentrations within the reactors and permitted the measured NO_x to be interpreted in terms of the four contributing mechanisms (Table 1).

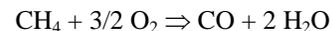
Novosselov [13] extended the database by running a wide range of lean-premixed combustion conditions, all for methane fuel, using chemical reactor networks (i.e., CRN modeling). The pressure was selected from 5 to 20 atm. The inlet air temperature was set assuming compression from 1 atm and 15 degrees C to the pressure of interest through a compressor of 85% efficiency. The chemical reactors and residence times used are cataloged in Table 2. This process yielded a large computer-generated database.

From these CRN computer runs, the results of value for developing the eight-step global mechanism are the following:

- Temperature: T (K).
- Concentrations ($kmol/m^3$) of major species and OH: CH_4 , CO, CO_2 , O_2 , H_2O , OH, and N_2 .
- Concentrations ($kmol/m^3$) of species involved in NO formation (see Table 1): CH, N_2O , NNH, O, H.
- Rates ($kmol/m^3\cdot s$) of CH_4 and CO oxidation, and dissociation of CO_2 .

The elemental rate data for Rxn's 1, 5, 6, 7, and 10 from GRI 3.0 are also required. Although Rxn 11 has recently received attention in the literature, e.g., [14], it is not included in this development since it is not part of GRI 3.0.

Step 1 in the eight-step mechanism is the oxidation of methane. The stoichiometry is expressed by the following chemical equation, and the CRN solutions provide the database for the CH_4 loss rate (oxidation rate) R_1 .



When evaluating the loss of hydrocarbon material in the CRN, our methodology is to include methyl radical (CH_3) with the CH_4 . For most cases run, other hydrocarbon containing species in the combustion field are negligibly small compared to CH_4 and CH_3 . (The global mechanism has not yet been designed to consider sub part per million levels of formaldehyde.)

Step 2 is the oxidation of CO. The stoichiometry is expressed by the following chemical equation, and the CRN solutions provide the database for the CO loss rate (oxidation rate) R_2



At the elemental level, this step occurs principally by the forward rate of the reaction:

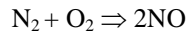


Step 3 is the dissociation of CO₂: The stoichiometry is expressed by the following chemical equation, and the CRN solutions provide the database for the CO₂ loss rate (dissociation rate) R₃.



At the elemental level, this step occurs principally by the reverse of the reaction $\text{CO} + \text{OH} \rightleftharpoons \text{CO}_2 + \text{H}$.

Step 4 is the major lumped route to flame-NO formation: the Zeldovich and nitrous oxide mechanisms operating within the flame zone. The stoichiometry is expressed by the following chemical equation:



The rate of NO formation is found from the CRN database per the rates of Table 1. This gives the step-4 rate as:

$$R_4 = 2k_1[\text{N}_2][\text{O}] + 2k_5[\text{N}_2\text{O}][\text{O}] + 2k_6[\text{N}_2\text{O}][\text{H}]$$

Step 5 is the second lumped route to flame-NO formation: the prompt and NNH mechanisms operating within the flame zone. The stoichiometry is again expressed by the chemical equation: $\text{N}_2 + \text{O}_2 \Rightarrow 2\text{NO}$.

The rate of NO formation is found from the CRN database per the rates of Table 1. This gives the step-5 rate as:

$$R_5 = 2k_7[\text{N}_2][\text{CH}] + 2k_{10}[\text{NNH}][\text{O}]$$

The species concentrations and temperature required for R₄ and R₅ are provided by the CRN solution.

So far, a large database of global rate data for R₁ through R₅ has been generated. This could be used via a look-up-table methodology in CFD computations. However, the goal here is to obtain global rate expressions for each of the five steps. This is explained after the three remaining steps of the mechanism are developed. The remaining steps (6-8) cover thermal NO formation; thus, they depend on equilibrium thermo-chemistry. These steps only involve the Zeldovich and nitrous oxide mechanisms, since only these survive into the post-flame zone. Furthermore, the thermal effect is subtracted from step 4 so that double counting doesn't occur. In all of these steps, the stoichiometry is expressed by the chemical equation from above: $\text{N}_2 + \text{O}_2 \Rightarrow 2\text{NO}$.

Step 6 accounts for H-atom attack on N₂O, where both the H-atom and N₂O are assumed to be at local equilibrium concentration. Thus, the rate is:

$$R_6 = 2k_6[\text{N}_2\text{O}]_e[\text{H}]_e$$

[N₂O]_e is expressed in terms of [N₂] and [O₂] and the equilibrium constant between N₂O, N₂, and O₂, and [H]_e is expressed in terms of [H₂O] and [O₂] and the equilibrium constant between H, H₂O, and O₂. The result of these manipulations, leading to the rate expression used, is given in Table 3. (Strictly, the N₂, O₂, and H₂O should also be denoted as

equilibrium concentrations, but under lean-premixed post-flame conditions, the difference between equilibrium and kinetic values for these major species is small.)

Step 7 accounts for O-atom attack on N₂O, where both the O-atom and N₂O are assumed to be at local equilibrium concentration. Thus, the rate is:

$$R_7 = 2k_5[\text{N}_2\text{O}]_e[\text{O}]_e$$

[O]_e is expressed in terms of [O₂] and the equilibrium constant between O and O₂. The result of the manipulations, leading to the rate expression used, is given in Table 3. Step 7 augmented by step 6 represents thermal nitrous oxide NO.

Step 8 accounts for O-atom attack on N₂, where the O-atom is assumed to be at local equilibrium concentration. Additionally, N-atom steady-state is assumed valid, and the reverse rates of the Zeldovich mechanism are assumed negligible (which is clearly valid for lean premixed combustion). This is textbook thermal Zeldovich NO (e.g., see [8]). The rate is:

$$R_8 = 2k_1[\text{N}_2][\text{O}]_e$$

The result of the manipulations, leading to the rate expression used, is given in Table 3.

The general equation used for the global reaction rates, R₁-R₅, is:

$$R = 10^{n+mP} [A]^{a+xP} [B]^{b+yP} [C]^{c+zP} \exp\{-(T_a+T_{a1}P)/T\}$$

where: T_a+T_{a1}P is the activation temperature (K)
T is the combustion temperature (K)
[] is the species concentration (kmol/m³)
P is pressure (atm)
R is reaction rate (kmol/m³-s)
n, m, a, b, c, x, y, z, T_a, and T_{a1} are coefficients and parameters to be determined

Regression analysis on the CRN database is performed to obtain the global rate expressions for R₁-R₅. Following selection of the species dependences for each global rate, the natural logarithm of the global rate expression is written and then least squares analysis is conducted to obtain the coefficients and parameters. The global rate expressions that give the best agreement to the CRN database are listed in Table 3 below. As a surrogate for the flame free radicals, CO is used (see Polifke et al. [15]). R₁, R₂, R₄, and R₅ depend on [CO]. As expected, R₁ (methane oxidation) also depends on [CH₄] and [O₂]. R₂ (CO oxidation) also depends on [H₂O] and [O₂], because of importance of the hydroxyl radical in the elementary chemistry. R₃ (CO₂ dissociation) is found to depend only on [CO₂]. Fine tuning of R₁ and R₂ has been conducted so that CO \rightleftharpoons CO₂ equilibrium can be obtained in the burnout zone of the combustor. The best fits for both flame-NO steps (R₄ and

R₅) depend on [CO] as a surrogate for the free radical chemistry, and [O₂].

Figure 9 provides an example of agreement between a global rate expression and the CRN database. In this case, R₅ is plotted (note: CH mechanism means prompt mechanism). As shown in Table 2, this case used the single PSR and two-PSRs-in-series CRN schemes. Post-flame CRN schemes were not used because CH and NNH do not survive the flame. Typically, expect for a few outlying points at low rates, the agreement is very good. Although developed for methane combustion, steps 2 through 8 should be valid when other gaseous fuels are burned in lean-premixed combustion turbines. However, the mechanism is not valid for 1 atm combustion, for which free radical concentrations increase. See Nicol et al. [5] for a 1 atm global mechanism for lean-premixed methane oxidation with NO formation.

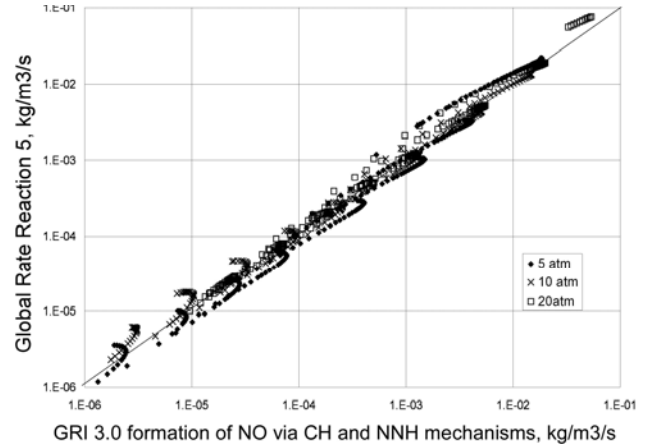


Figure 9. Comparison of R₅ by global rate expression of Table 3 (y-axis) vs. rates computed by GRI 3.0 (x-axis).

Table 2. Chemical reactor (CRN) schemes and residence times used in developing the eight-step mechanism.

Reactor Schemes (adiabatic)	CH ₄ Oxidation	CO Oxidation	CO ₂ Dissociation	Flame NO by Zeld & N ₂ O	Flame NO by Prompt & NNH
PSR: blowout to 3 millisecc (ms)	X	X	X	X	X
PSR at blowout + PSR to 3 ms	X	X		X	X
PSR from blowout to 3 ms + PFR to 3 ms				X	
PSR from blowout to 3 ms + PFR approaching CO⇌CO ₂ equilibrium		X	X		
PSR from blowout to 3 ms + PFR with air addition approaching CO⇌CO ₂ equil.		X	X		

Table 3. Eight-step global mechanism for lean-premixed combustion in industrial gas turbine engines.

CH ₄ + 3/2O ₂ ⇒ CO + 2H ₂ O
$R_1 = 10^{13.354 - 0.004628P} [\text{CH}_4]^{1.3 - 0.01148P} [\text{O}_2]^{0.01426} [\text{CO}]^{0.1987} \exp\{-(-21932 + 269.4P)/T\}$
CO + 1/2O ₂ ⇒ CO ₂
$R_2 = 10^{14.338 + 0.1091P} [\text{CO}]^{1.359 - 0.0109P} [\text{H}_2\text{O}]^{0.0912 + 0.0909P} [\text{O}_2]^{0.891 + 0.0127P} \exp\{-(-22398 + 75.1P)/T\}$
CO ₂ ⇒ CO + 1/2O ₂
$R_3 = 10^{15.8144 - 0.07163P} [\text{CO}_2] \exp\{-(-64925.8 - 334.31P)/T\}$
N ₂ + O ₂ ⇒ 2NO (flame-NO by Zeldovich and nitrous oxide mechanisms)
$R_4 = 10^{14.122 + 0.0376P} [\text{CO}]^{0.8888 - 0.0006P} [\text{O}_2]^{1.1805 + 0.0344P} \exp\{-(-46748 + 126.6P)/T\}$
N ₂ + O ₂ ⇒ 2NO (flame-NO by prompt and NNH mechanisms)
$R_5 = 10^{29.8327 - 4.7822\log(P)} [\text{CO}]^{2.7911 - 0.04880P} [\text{O}_2]^{2.4613} \exp\{-(-61265 + 704.7P)/T\}$ §
N ₂ + O ₂ ⇒ 2NO (thermal-NO by H-atom attack on N ₂ O)
$R_6 = 10^{14.592} [\text{N}_2] [\text{H}_2\text{O}]^{0.5} [\text{O}_2]^{0.25} T^{-0.7} \exp(-69158/T)$
N ₂ + O ₂ ⇒ 2NO (thermal-NO by O-atom attack on N ₂ O)
$R_7 = 10^{10.317} [\text{N}_2] [\text{O}_2] \exp(-52861/T)$
N ₂ + O ₂ ⇒ 2NO (thermal-NO by O-atom attack on N ₂)
$R_8 = 10^{14.967} [\text{N}_2] [\text{O}_2]^{0.5} T^{-0.5} \exp(-68899/T)$

§ log = log base 10

APPLICATION TO BLUFF BODY COMBUSTOR

The high-pressure, lean-premixed, methane-fired, bluff body combustor of Bucher et al. [16] is modeled with CFD and the eight-step global mechanism. Figure 10 shows the cross-sectional area of the actual combustion chamber viewed from the exit plane, where the gas sampling probe is located. Two-dimensional CFD simulations of the combustor are shown in Figures 11-14. Premixed methane and air enter at the left of Figures 11-14, flow through the channel along the top of the bluff body (the bottom channel is not shown), enter the combustion chamber, and create a large recirculation zone at the base of the bluff body (as indicated by the region of low velocity magnitude in Figure 11). The blockage ratio created by the bluff body is 0.63. The inlet air temperature and pressure are 678 K and 14.3 atm, respectively, and the nominal air mass flow rate is 1.08 kg/s. The air is split between the main air (that is, the premixer air) and the combustor wall cooling air. Impingement/effusion cooling is used. Bluff body cooling air is drawn from the main air. Most of the methane is premixed into the main air well upstream of the channels running along the bluff body – see Bucher et al. [16]. Additionally, a few percent of the methane is injected via small jets located at the corners of the bluff body. Although the eight-step mechanism has not been designed to model stoichiometric (and near-stoichiometric) combustion of fuel jets, the impact of using the eight-step mechanism outside of its range is very small in this case, because of the small percentage of pilot fuel burned.

The two-dimensional CFD simulations, Figures 11-14, of the upper half of the combustor extend from combustor inlet to outlet. The position of the flame zone is best indicated in Figure 12, as the temperature rapidly increases from that of the fuel-air mixture up to combustion temperature, and in Figure 13, as the zone of peak CO concentration. This is one of the leaner cases treated: pre-mixer ϕ is 0.59. The CFD indicates a flame zone starting near the bluff body corner and extending to the upper wall. Significant CO (1-2% by mole) is computed in the flame zone. At the exit plane, the CFD indicates a large CO concentration near the wall (because of the leanness of this case, the wall CO at the exit appears to be caused by effusion air quenching of flame CO). This CO falls rapidly as the wall region is departed. Nitric oxide is found spread across most of the combustor vertical dimension, though the concentration is greatest in the center and falls to zero at the air cooled wall. See Figure 14.

Maximum NO formation rate occurs in the flame zone. Peak flame-NO rates are: $2.2E-3 \text{ kmol/m}^3\text{-s}$ by step-4 and $1.8E-4 \text{ kmol/m}^3\text{-s}$ by step 5. Peak thermal-NO rates in the post flame zone are: $2.6E-5 \text{ kmol/m}^3\text{-s}$ by step-7 and $3.5E-5 \text{ kmol/m}^3\text{-s}$ by step-8.

The CFD modeling of the bluff body combustor is performed with the following assumptions and conditions as listed in Table 4.

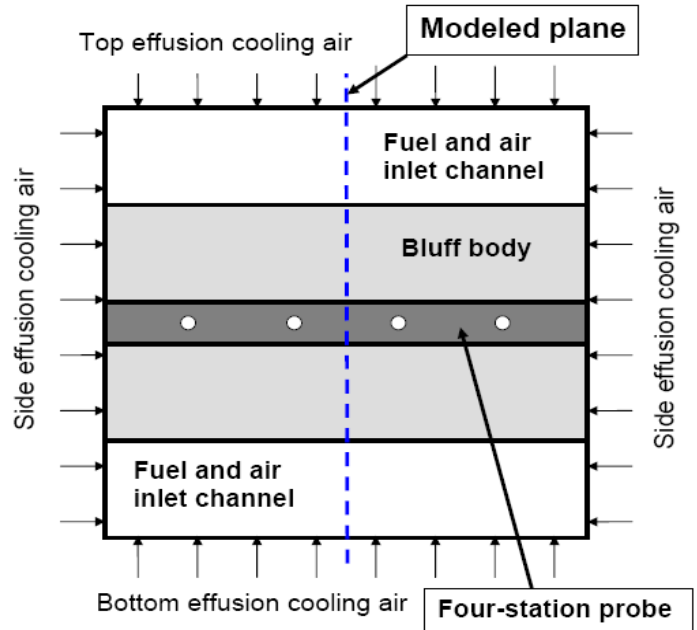


Figure 10. View of bluff body combustor from exit plane. Shown is the gas sampling probe.

Table 4. Modeling assumptions and boundary conditions.

Computational domain	2-D unstructured grid with 110,000 cells
Solver	Segregated RANS with species transport and volumetric reactions
Turbulence closure	Reynolds stress model
Convergence scheme	Second order (QUICK)
Pressure velocity coupling	Pressure implicit splitting of operators (PISO)
Wall treatment	Standard wall function
Heat loss	Convection and radiation heat transfer for top wall
Radiation heat transfer	Discrete ordinates (DO) model
Chemical kinetic rates	Eight-step mechanism
Chemical mixing rates	Eddy breakup rates

When modeling the combustor in 2-D rather than 3-D, it is necessary to make adjustments in the wall cooling. Effusion slots are modeled rather than effusion holes. Since there are no side walls in the 2-D modeling, only two surfaces receive cooling air: most of the cooling air acts on the top surface of the combustor, while a smaller amount is used to cool the base of the bluff body. Unless the ratio of cooling air to main air is reduced, too much air will cool the top surface and possibly quench the flame. This reduction in cooling air acts to maintain the ϕ of the flame zone to that of the actual combustor, but increases the ϕ of the post-flame zone and the overall ϕ of the modeled combustor.

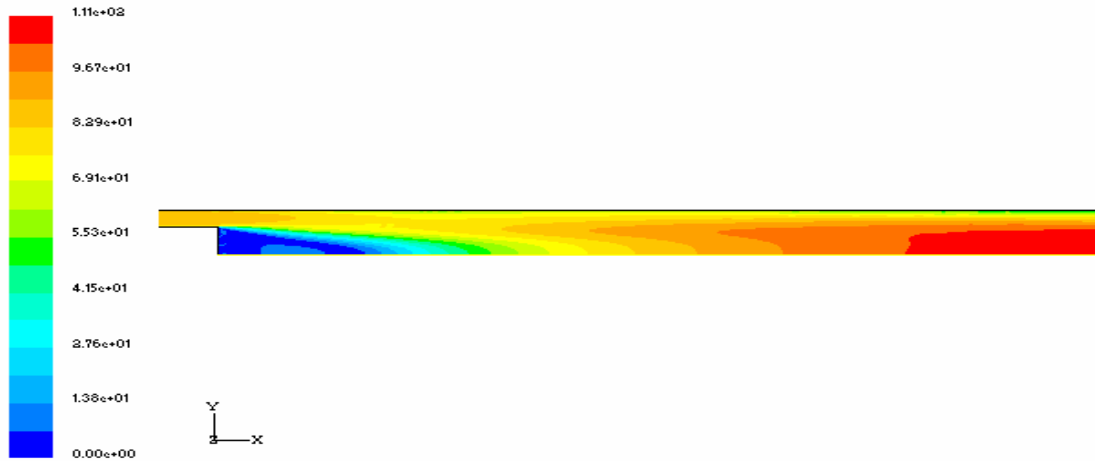


Figure 11. CFD solution for bluff body combustor velocity magnitude contours (m/s).

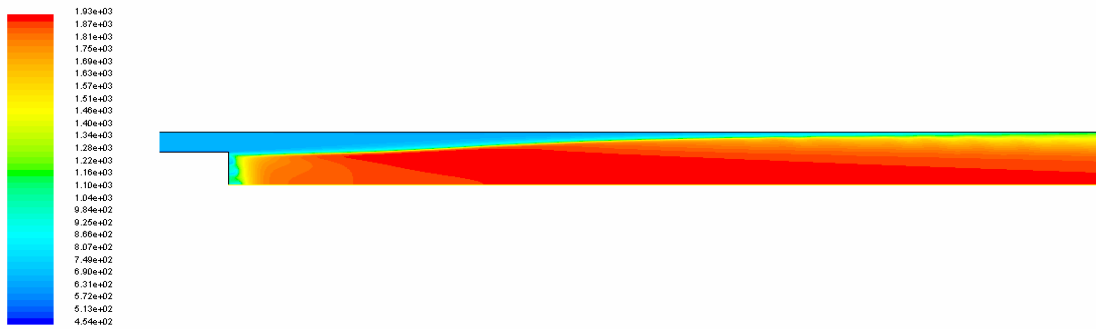


Figure 12. CFD solution for bluff body combustor temperature; maximum 1930K.

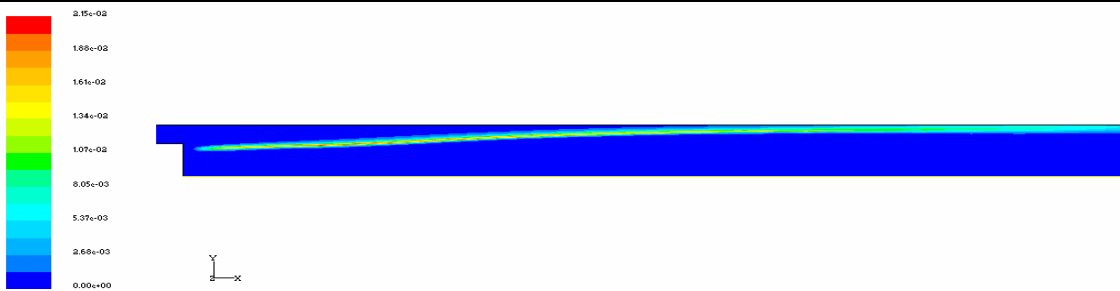


Figure 13. CFD solution for bluff body combustor CO mole fraction; maximum 2.15%, wet basis, actual O₂.

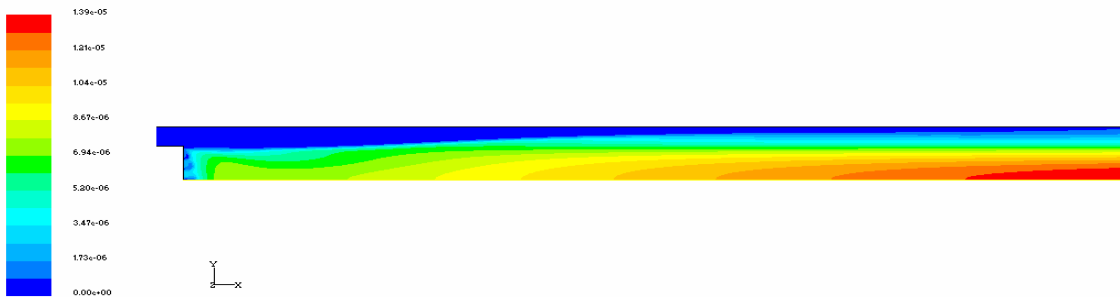


Figure 14. CFD solution for bluff body combustor NO mole fraction; maximum 13.9 ppmv, wet basis, actual O₂.

Modeling and measurement of CO are compared in Figure 15. When the premixer phi is less than 0.63, the CFD-area-average CO is considerably greater than the CFD-centerline CO. This is the situation depicted in Figure 13. For greater premixer phi's, however, and thus, for greater combustion temperatures, the two CFD CO results converge, and then, for the highest phi's run, the centerline CO exceeds the area-average CO. Now, the CO is caused by dissociation of CO₂, leading to enhanced CO in the hot gases found in the center of the combustor. For the highest phi's, the CO emission is thermodynamically controlled, whereas at the lower phi's it is kinetically controlled.

For the leanest phi's, the experimental CO is seen to lie at about 1/3 height between the centerline CFD result (which is very small) and the area-average CFD result (which is significantly influenced by the large amount of CO near the upper wall). This suggests the following relation for weighting the CFD results to the probe:

$$CO_{probe} \cong 0.7CO_{center} + 0.3CO_{average}$$

Novosselov [6] finds similar coefficients by considering diffusion of gas from the combustor wall towards the probe.

For the highest phi's examined, experimental CO is about 25 ppmv (dry 15% O₂), whereas the CFD results are in the 50-80 ppmv range (dry 15% O₂). Very likely, the difference is caused by enhanced dissociation of CO₂ in the post-flame zone of the 2-D CFD combustor, which as argued above may run hotter than the experimental combustor. Additionally, the opportunity for oxidation of the experimental CO cannot be ruled out as the hot combustion gases are drawn into the sampling probe and dwell there.

The comparison of modeling and measurement of NO_x are shown in Figure 16. The measured NO_x of Bucher et al. [16] is seen to increase smoothly from 8-10 ppmv (dry 15% O₂) at the leanest case (phi of 0.56) up to 30 ppmv (dry 15% O₂) at the highest phi plotted (0.69). As shown first by Bucher et al. [16], the experimental NO_x can be modeled closely using the correlation of Leonard and Stegmaier [17]. Leonard and Stegmaier operated a porous-plate burner over a wide range of lean-premixed conditions (including elevated pressures) up to about 10 ppmv NO_x (dry 15% O₂) and 1950 K, and showed NO_x emission correlating well with a single variable: adiabatic equilibrium flame temperature. This approach is used in deriving the L&S curves in Figure 16. For "L&S high", the front-end phi (which is based on the premixer phi plus the small corner jets' fuel), inlet air and fuel temperatures, and pressure are used to calculate the adiabatic equilibrium flame temperature. Then, the NO_x is determined from the Leonard and Stegmaier straight-line fit, of form:

$$\ln(NO_x) = a + bT$$

For "L&S low" in Figure 16, the front-end phi is adjusted by adding cooling air from the top wall, up to the point where

the flame approaches the wall. The effect of this is to decrease the flame temperature and the L&S NO_x. The L&S NO_x curves are truncated once they exceed the range of the Leonard and Stegmaier NO_x database.

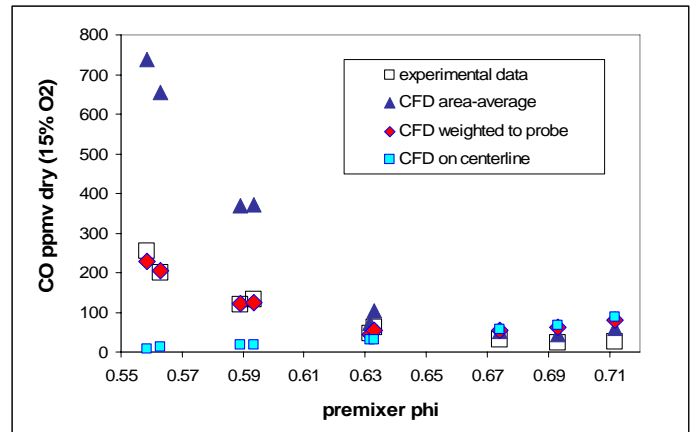


Figure 15. CFD results for CO in comparison to measurements for bluff body combustor.

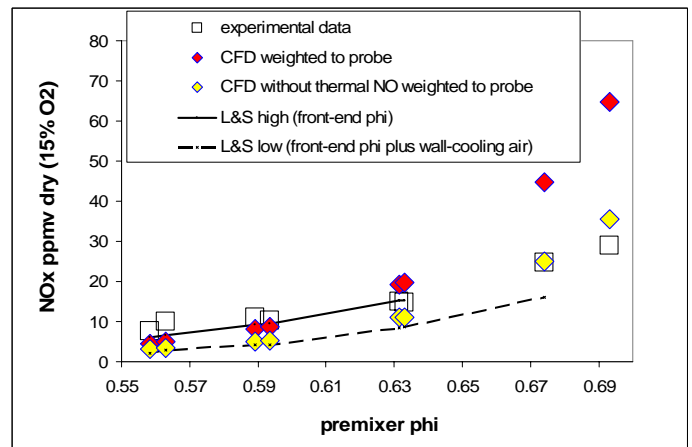


Figure 16. CFD results for NO in comparison to measurements for bluff body combustor. Calculations of Leonard and Stegmaier NO_x also plotted.

Figure 16 also shows the CFD generated NO results. The procedure is the same as used for the CO, that is, the centerline and area-average 2-D CFD results for NO are generated. These values are then multiplied respectively by 0.7 and 0.3 and added to give the probe NO. The CFD-probe NO is significantly less sensitive to the choice of the coefficients (so long as they add to one) than the case of CO for the lean mixtures.

The Figure 16 CFD results also include the effect of turbulent fluctuations on NO formation. This follows from a separate CFD study of lean-premixed combustion using PDF modeling (Novosselov [6]), from which it is deduced that for the leanest phi's an additional 20-25% NO could form, and for the highest phi's, the increase could be 10-15%. This implies a

greater impact of turbulent fluctuations, and thus, a larger correction to the steady-state NO, for flame-NO than for thermal-NO in lean-premixed combustors.

Two sets of CFD NO results are plotted in Figure 16: the upper one for all NO steps included, and the lower one with the thermal NO steps removed.

The following observations are drawn:

- The 2-D CFD-simulated NO, using all steps, shows reasonably close agreement to the experimental NO_x when the premixer phi is less than about 0.63.
- For the highest values of phi examined, the CFD, using all steps, over-predicts the measured NO_x. The over-prediction is in the thermal NO, presumably because the post-flame zone of the 2-D combustor may run hotter than the actual combustor.
- The CFD solution with the thermal NO steps removed, forming only flame-NO by steps 4 and 5, shows good agreement with “L&S low” over the range of validity of the Leonard and Stegmaier NO_x.

APPLICATION TO GAS TURBINE COMBUSTOR

Above in this paper we showed CFD results for a generic, lean-premixed, gas turbine combustor. In that modeling a 2-D structured grid of 31,000 cells was used. The Reynolds stress turbulence closure model with quadratic pressure strain was used; other conditions were similar to those listed in Table 4 for the bluff body combustor.

Additionally, lean-premixed, engine test rig combustors have been modeled by multiple-element chemical reactor network (CRN) models. The development of a 31-element CRN for an annular test rig combustor with air back-side cooling is reported in the 2006 paper by Novoselov et al. [18]. The development of the 31-element CRN is based on 3-D CFD solution of a sector of the annular combustor. The CFD solution provides insight and information useful for selecting the size and nature of the CRN elements and mass exchange between the elements. The CRN can treat either uniform or non-uniform fuel-air ratio profiles at the premixer-injector outlet and takes into account velocity non-uniformity at the premixer outlet. It can also treat premixed pilot flames. The 3-D CFD uses the eight-step mechanism. On the other hand, the CRN is capable of quickly running either a full chemical kinetic package (GRI 3.0 in this study) or a global mechanism (the eight-step global mechanism in this study).

The 3-D CFD solutions have been used mainly to guide the CRN development, whereas the CRN output contains the useful information for comparison of the eight-step predictions of CO and NO_x to those of full GRI 3.0 solutions and the engine test rig data.

Table 5 shows the CO comparison and Figure 17 shows the NO_x comparison. The eight-step mechanism shows very good agreement to the full GRI 3.0 mechanism for CO and NO_x emission calculations when applied to the industrial gas turbine combustor through the 31-element CRN. The slightly greater amount of NO_x (actually NO) obtained with the eight-

step mechanism is the result of slightly higher combustion temperature obtained with the global chemistry compared to GRI 3.0. That is, the full mechanism has somewhat more endothermicity that is lacking in the global mechanism. This deficiency can be overcome easily by adding a small amount of an inert species to the methane used with the global mechanism. Both mechanisms show very good agreement to the NO_x measured for the engine test rig combustor. This provides confidence in the 31-element CRN, which was the objective of the paper by Novoselov et al. [18], and confidence in the eight-step mechanism, which is the purpose of the current paper.

Table 5. Comparison of CO Emissions for Test Rig Combustor Running Lean Premixed [18].

Pilot Level	35-185% of neutral
GRI 3.0 in CRN	1.82 ± 0.03 ppmv (dry 15% O ₂)
8-step in CRN	1.96 ± 0.03 ppmv (dry 15% O ₂)
The CO emissions measured for the engine test rig are within a few ppmv of the CRN calculations.	

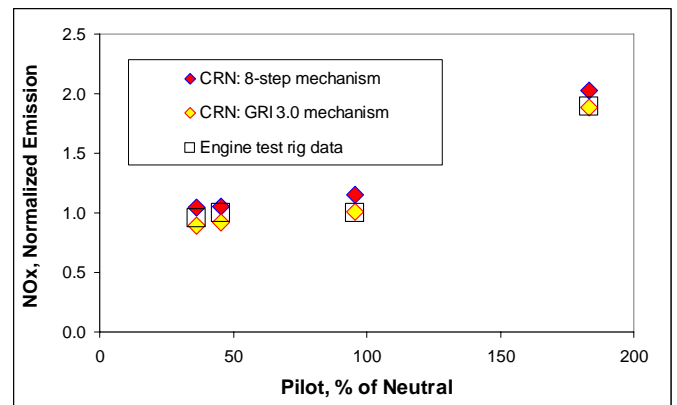


Figure 17. Comparison of modeled and measured NO_x for the engine test rig combustor. NO_x emission is normalized by test rig emission for the neutral pilot. At neutral, the pilot has the same phi as the main premixer.

CONCLUSIONS

In this paper the development of the eight-step mechanism for methane oxidation with flame and post-flame NO formation for lean-premixed, high-pressure combustion is explained. The eight steps are given. In addition to dominance by flame-NO, a thermal nitrous oxide step is shown to form essentially equal amounts of NO to thermal Zeldovich NO in the post-flame zone. The range of validity of the eight-step mechanism is 5-20 atm pressure, air inlet temperature corresponding to compression to this pressure range, and 0.45 to 0.75 phi. Combustors with pilot flames of phi somewhat greater than 0.75 have been modeled with the mechanism, but since this is outside of the development range, the percentage of pilot fuel burned should be small, otherwise inaccuracies may occur in the computed NO emission. Two gas turbine lean-premixed

combustors, one a virtual generic combustor, and the other an engine test rig combustor, have been modeled with the eight-step mechanism using both CFD and CRN techniques. CFD modeling of the generic combustor is used to show how and where NO forms in single-digit NO_x combustors. Modeling of the test rig combustor shows very good agreement to the measured CO and NO_x, especially the NO_x. This provides confidence in the eight-step mechanism. A bluff body combustor is also modeled in CFD using the eight-step mechanism, with modeling results comparing favorably to the measurements of CO and NO_x. Nonetheless, this combustor has presented a challenge when comparing modeling with measurement, because of the non-uniformity of the exit plane gas composition.

Next topics for work include application of the eight-step mechanism to other databases for lean-premixed combustion, and development of the mechanism for alternative gaseous fuels of interest for gas turbine engines, including natural gas high in NMHC, LNG, syngases, and syngases and hydrogen blended with natural gas.

ACKNOWLEDGEMENT

This paper is based on the PhD thesis of Dr. Igor Novosselov [6].

REFERENCES

- 1 Westbrook, C. K. and Dryer, F. L., *Combust Sci and Technol*, vol 27, pp 31-43 (1981).
- 2 Westbrook, C. K. and Dryer, F. L., *Prog. in Energy and Combust Sci*, vol 10, pp 1-57 (1984).
- 3 DuPont, V., Pourkashanian, M., and Williams, A., *Journ of the Institute of Energy*, vol 66, p 20 (1993).
- 4 Hautman, D. J., Dryer, F. L., Schug, K. P., and Glassman, I., *Combust Sci and Technol*, vol 25, pp 219-235 (1981).
- 5 Nicol, D.G., Malte, P.C., Hamer, A.J., Roby, R.J., and Steele, R.C., *Journ of Engr for Gas Turbines and Power, Trans of ASME*, vol. 121, pp 272-280 (1999),
- 6 Novosselov, I.V., "Chemical Reactor Network Modeling of Combustion Systems," *Ph.D. Dissertation, University of Washington*, Seattle, WA (2006). (This may be accessed online at the address www.energy.washington.edu, denoting "laboratory," followed by "publications.")
- 7 Magnussen, B. F. and Hjertager, B. H., "On Mathematical Models of Turbulent Combustion with Special Emphasis on Soot Formation and Combustion," *Proceedings Sixteen Symposium (International) on Combustion*, pp 719-729, *The Combustion Institute*, Pittsburgh, PA (1977).
- 8 Heywood, J. B. "Internal Combustion Engine Fundamentals," McGraw-Hill (1988).
- 9 Rutar-Shuman, T., "NO_x and CO Formation for Lean-Premixed Methane-Air Combustion in a Jet-Stirred Reactor Operated at Elevated Pressure," *Ph.D. Dissertation, University of Washington*, Seattle, WA (2000).
- 10 Bengtsson, K. U. M., "Experimental and Numerical Study of the NO_x Formation in High-Pressure Lean Premixed Combustion of Methane," *PhD Thesis, Swiss Federal Institute of Technology*, Zürich, Switzerland (1998).
- 11 Rutar, T. and Malte, P.C., *ASME Journ of Engr for Gas Turbines and Power*, vol 124, pp 776-783 (2002).
- 12 GRI MECH 3.0. World Wide Web Site http://www.me.berkeley.edu/gri_mech/ accessed 2005.
- 13 Novosselov, I.V., "Eight-Step Global Kinetic Mechanism of Methane Oxidation with Nitric Oxide Formation for Lean Premixed Combustion Turbines." *MSME Thesis, University of Washington*, Seattle, WA (2002). (This may be accessed online at the address www.energy.washington.edu, denoting "laboratory," followed by "publications.")
- 14 Konnov, A.A., De Ruyck, J., *Combust. Flame*, vol 125, p 1258 (2001).
- 15 Polifke, W., Dobbeling, K., Sattelmayer, T., Nicol, D.G., and Malte P.C., *Transactions of ASME, Journ of Engr for Gas Turbines and Power*, vol 118, pp 765-772 (1996).
- 16 Bucher, J., Edmonds, R.G., Steele, R.C., Kendrick, D.W., Chenevert, B.C., and Malte, P.C., "The Development of a Lean-Premixed Trapped Vortex Combustor," Paper No. GT-2003-38236, *ASME International Gas Turbine and Aeroengine Congress*, Atlanta, GA (2003).
- 17 Leonard, G. and Stegmaier, J., *ASME Journ of Engr for Gas Turbines and Power*, vol 116, pp 542-546 (1994).
- 18 Novosselov, I.V., Malte, P.C., Yuan, S., Srinivasan, R.; and Lee, J.C.Y. "Chemical Reactor Network Application to Emissions Prediction for Industrial DLE Gas Turbine," Paper No. GT2006-90282, *ASME International Gas Turbine and Aeroengine Congress*, Barcelona, Spain (2006).